JOURNAL OF Applied Polymer SCIENCE

Chemical and mechanical degradation of silicone rubber under two compression loads in simulated proton-exchange membrane fuel-cell environments

Zhiqiang Wang, Jinzhu Tan, Yankang Wang, Zenghui Liu, Qiuyue Feng
School of Mechanical and Power Engineering, Nanjing Tech University, Nanjing, Jiangsu 211816, China
Correspondence to: J. Tan (E-mail: tjznjut@njtech.edu.cn)

ABSTRACT: Long-term chemical and mechanical stability of gaskets in proton-exchange membrane (PEM) fuel cells is critical to the sealing and normal operation of these fuel cells. In this study, the chemical and mechanical degradation of a silicone rubber was investigated. Two compression loads and two simulated environments were used. The weight change of sample was monitored. Optical microscopy was applied to observe the morphological changes on the specimen surface. Attenuated total reflection (ATR)–Fourier transform infrared (FTIR) spectroscopy and X-ray photoelectron spectroscopy (XPS) were used to investigate the chemical changes on the surface of specimens after exposure to the simulated solutions and subjection to compression loads over time. A compression stress-relaxation test was used to elucidate the stress-relaxation property changes of the specimens after exposure to the simulated fuel-cell environments and the compression loads. Optical microscopy showed that the surface morphology of the specimens changed from initially smooth to slightly rough followed by crack initiation and finally propagation. The ATR–FTIR and XPS results indicate that the surface chemistry of the specimens significantly changed via decrosslinking and chain scission after exposure to the simulated environments and compression loads over time. The compression stress-relaxation test results indicate that the mechanical properties of the silicone rubber specimens changed significantly. We found that both the acid concentration of the test solution and the compression load significantly affected the degradation of the silicone rubber material. © 2019 Wiley Periodicals, Inc. J. Appl. Polym. Sci. **2019**, *136*, 47855.

KEYWORDS: aging; batteries and fuel cells; degradation; elastomers; mechanical properties

Received 19 September 2018; accepted 28 March 2019
DOI: 10.1002/app.47855

INTRODUCTION

Proton-exchange membrane (PEM) fuel cells are considered to be one of the cleanest energy source systems for automotive applications and residential power sources in the 21st century because of their high efficiency, near-zero emissions, quiet operation, quick startup, and high power density.[1,2] A single PEM fuel cell contains many components, including end plates, current collectors, bipolar plates, elastomeric gaskets, gas-diffusion layers, and a membrane electrode assembly. Among them, the gasket as an indispensable component is used to make the cathode and anode reactant gases (H_2 and O_2/air) stay in the area. Because the gasket materials are exposed to a humid acidic environment for a long time and are always subjected to a compression load, they can easily degrade or lose their sealing performance during PEM fuel-cell operation. In addition, to maintain all components inside the fuel cells in good contact, the gasket material should be flexible. Once the gasket fails (e.g., via relaxation or hardening) in fuel cells, it may lose its sealing ability, and this can cause the leakage of reactant gases. The mixing of leaked gases may seriously influence the durability and lifetime of the fuel cells.[3,4] Furthermore, the calcium and magnesium leached because of the damage to the gaskets may pollute the cell and reduce its voltage and durability.[5,6] Therefore, the stability of gasket materials plays an important role in the durability and performance of PEM fuel cells during operation.[7]

Silicone rubber materials have the following advantages: high- and low-temperature resistance, insulation properties, nontoxicity, and low cost. They are widely used in various industrial applications, including fuel cells.[8] In the open literature, many researchers have discussed the damage process of elastomeric materials in different environments. Mitra *et al.*[9,10] investigated the chemical degradation of two Ethylene-Propylene-Diene-Monomer (EPDM) rubbers, which had different molar masses and chain branching under an acidic environment, and their results show that both the molar mass and chain branching had direct impacts on the materials' chemical degradation. Kim and Kim[11] did a comparative analysis of the characteristics of surface wettability and recovery ability

between EPDM and silicone rubber as sealing materials in PEM fuel cells. The degradation processes of silicone rubbers with different hardnesses and subjected to simulated environments of fuel cells was reported by Feng *et al.*[12] Li *et al.*[13] also studied the degradation of silicone rubbers with different hardnesses subjected to cathode outlet solutions. Chang *et al.*[14] discussed the effects of the temperature and humidity on the aging properties of silicone rubber materials. Cui and coworkers[15–17] reported that water obviously affected the life of liquid-silicone rubber seals and conducted a life prediction of liquid-silicone rubber. Their test results show that water significantly accelerated the stress relaxation of the materials at higher temperatures. Kim *et al.*[18] investigated the effects of acid–heat aging on the performance of rubber gaskets for fuel cells and predicted the useful life of the rubber gaskets. Tan and coworkers[19–21] studied the chemical degradation of different elastomeric materials (i.e., EPDM, fluoroelastomer, and silicone rubber material) after exposure to simulated PEM fuel-cell environments. The effect of the temperature on the mechanical properties of silicone rubber was experimentally studied by Rey *et al.*[22] Schulze *et al.*[8] reported that the release of small particles from silicone rubber during the operation of PEM fuel cells ultimately affected their performance. Li *et al.*[23] reported the chemical degradation of silicone rubber material exposed to several accelerated test solutions for a period of time. Liu *et al.*[24] investigated the effect of a silane coupling agent as an additive on the sealing performance of silicone rubber. Millichamp *et al.*[25] published a review on the mechanisms and effects of mechanical compression on PEM fuel cells.

Although there is a lot of discussion in the literature on the damage process and changes in the mechanical properties of elastomeric materials, few researchers have reported on the damage process and damage mechanism of elastomeric materials both in PEM fuel-cell environments and under compression loads. It is well known that the sealing gaskets are always compressed and under a certain pressure in PEM fuel cells. Therefore, the level of compression stress directly determines the sealing effect of the gasket. Mechanical compression is a big challenge for ensuring effective performance and durability during long-term PEM fuel-cell operation.

In this study, the chemical and mechanical degradation of a silicone rubber material after exposure to simulated environments and two compression loads (i.e., 0.13 or 0.26 MPa) were studied. In this study, we attempted to examine the degree of damage and damage mechanism of silicone rubber specimens under different compression loads in simulated fuel-cell environments. These results may help component manufacturers to assess the impact of the design or material selection on PEM fuel-cell performance. Two compression loads (i.e., 0.13 and 0.26 MPa) were applied to the specimens to simulate the actual load during fuel-cell operation and to accelerate the stress test. Two simulated solutions [i.e., a regular solution (RS) and an accelerated durability test (ADT) solution] were prepared. The first solution (i.e., RS) was close to the real environment inside the fuel cell. The second solution (i.e., ADT solution) was an aggressive solution for short-term accelerated aging tests. The surface morphological changes in the aged specimens were observed with optical microscopy. Attenuated total reflection (ATR)–Fourier transform infrared (FTIR) spectroscopy and X-ray photoelectron spectroscopy (XPS) were conducted to detect chemical changes in the specimen surface. Compression stress-relaxation measurements were performed to assess the mechanical property changes in the silicone rubber material before and after exposure to simulated environments and different compression loads.

EXPERIMENTAL

Materials and Simulated Fuel-Cell Environments

A methyl vinyl silicone rubber material was used in this study, and the percentage of vinyl in the basic rubber was 0.13%. Fumed silica (ZH909) was used as a reinforcing agent to improve the strength of the silicone rubber material. Hydroxyl silicone oil (JS209) as a structural control agent and dicumyl peroxide as a good curing agent were added to the basic rubber. The silicone rubber elastomeric material was fabricated with a curing temperature of 160 °C, a molding pressure of 10 MPa, and a molding time of 25 min.

Two solutions were used in this study. The first solution, which was the same was the actual solution in PEM fuel cells was named RS. Concentrations of 98% H_2SO_4 and 48% HF were dissolved in deionized water. The final composition of RS was 12.5 ppm H_2SO_4, 1.8 ppm HF, and deionized water. The RS pH was close to 3.4.[21] The second solution had a higher acid concentration in this study and was named the ADT solution. It was also made with 98% H_2SO_4 and 48% HF dissolved in deionized water. The final composition was 1 *M* H_2SO_4, 1.8 ppm HF, and deionized water. The deionized water in both the RS and ADT solution had an 18 MΩ resistance.

The test temperature was 80 °C to simulate the actual temperature during PEM fuel-cell operation.

Aging and Characterization Methods

A silicone rubber elastomeric material was fabricated in this study. The test specimens prepared were 15 mm in length, 15 mm in width, and 2 mm in thickness. The specimens were sandwiched between two polytetrafluoroethylene (PTFE) plates. Two dead weights were applied to the test specimens to provide compression stresses of 0.13 and 0.26 MPa, respectively. The compression stress of 0.13 MPa was close to the actual operating load in a single PEM fuel cell.[26,27] The compression load of 0.26 MPa was used for the accelerating stress test. The sample and fixture were put into a big PTFE bottle containing the test solution, as shown in Figure 1. The PTFE bottle was placed in an oven, and an oven temperature of 80 °C was selected. Then, the test specimens were taken out at the required time. The specimen weight changes were recorded with a microelectronic balance with resolution of 0.1 mg. The surface morphological change of the specimens after exposure to simulated solutions and subjected to compression loads were observed with an optical microscope (ZMM-300).

ATR–FTIR spectroscopy was used to investigate the chemical change on the surface of specimen with an IRAFFINITY-1S instrument (Shimadzu Corp., Japan). The spectra were recorded at a resolution of 0.1 cm^{-1}. XPS analysis was conducted to investigate the chemical damage of specimens with a Thermo-Fisher Scientific K-Alpha spectrometer with monochromatic Al Kα X-ray source. The high-resolution XPS analysis were also performed in the silicone 2p (Si2p) and oxygen 1s (O1s) regions. Note that to ensure the accuracy of all of the test results, the degraded specimens were

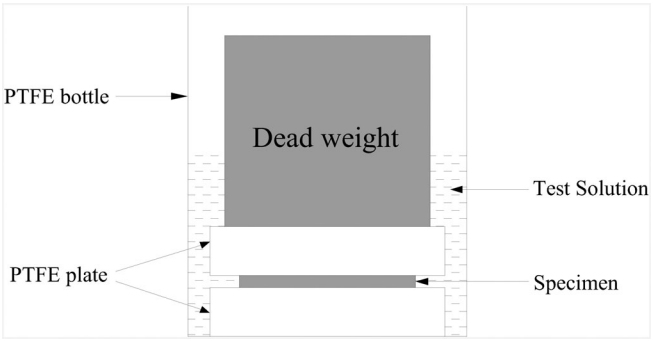

Figure 1. Schematic representation for tests under the compression load.

thoroughly rinsed with deionized water to remove the residual acids from the specimens. The specimens were dried in air for further analysis.

The compression stress-relaxation tests of the silicone rubber elastomeric material were conducted according to ISO 3384:2005. Cylindrical specimens were prepared for the compression stress-relaxation test, and the specimens had dimensions of 13 ± 0.5 mm in diameter and 6.3 ± 0.3 mm in height. The tests were performed in ambient air at a strain level of 25% with a universal instrument (MZ4000, MingZhu Instruments, Ltd., China). The computer was used to automatically measure and record the forces and time, and the stress-relaxation decay rate was calculated with eq. (1):

$$\text{Stress}-\text{relaxation decay rate} = E_t/E_0 \times 100\% \quad (1)$$

where E_0 is the stress when the strain just reaches 25% and E_t is the stress at time t.

RESULTS AND DISCUSSION

Weight Change

The specimens were taken out if the simulated environments at selected times. The weight change in the specimens was monitored after the specimens were thoroughly cleaned with deionized water and dried at room temperature for 24 h. The percentage weight loss (W_L) for the degraded specimen was calculated as follows:

$$W_L = \frac{W_2 - W_1}{W_1} \times 100\% \quad (2)$$

where W_1 is the initial weight of specimen (i.e., before exposure) and W_2 is the weight of the tested specimen (i.e., after exposure).

Figure 2 shows the weight loss of the specimens with exposure time under a 0.13 or 0.26 MPa compression load in the RS or ADT solution. The results in Figure 2 indicate that all of the specimens lost weight gradually with exposure time. Furthermore, with increasing acid concentration of the test solution, the weight loss of the specimen became more under identical the compression load (i.e., 0.13 or 0.26 MPa). As also shown in Figure 2, the weight loss for the specimen under the 0.26 MPa compression load was obviously greater than that for the specimen subjected

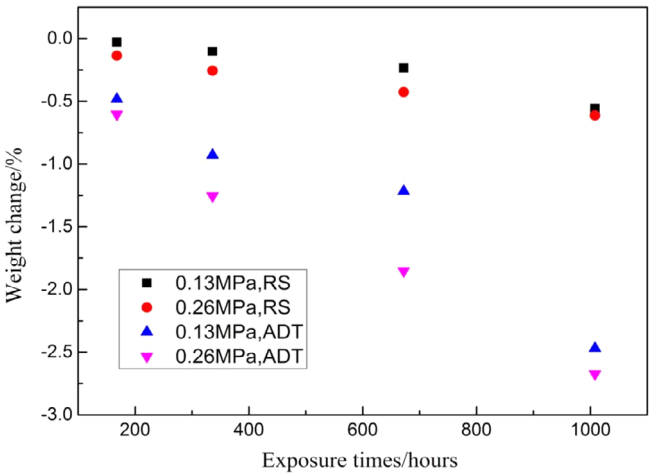

Figure 2. Weight loss with the exposure time for the test samples subjected to compression loads in the simulated PEM fuel-cell environments. [Color figure can be viewed at wileyonlinelibrary.com]

to the 0.13 MPa compression load in the same test solution (i.e., the RS or ADT solution); this reflected the impact of the mechanical compression load.

The weight loss results were consistent with our previous study,[26] in which the specimens were only subjected to one compression load and were exposed to ADT solution.

Overall, from the weight loss tests, we concluded that

1. The exposure time, exposure environment, and compression load had important effects on the weight loss.
2. The acid concentration and compression load significantly affected the weight loss; that is, the silicone rubber specimen had a greater weight loss under more acidic concentrations and/or with more compression stress.
3. The effect of the compression load on the weight loss of the specimen was more pronounced in the ADT solution.

Microscopy

Optical microscopy was conducted to detect the surface morphologies of the silicone rubber specimens in the simulated solutions (i.e., RS or ADT solution) and subjected to various compression loads (i.e., 0.13 or 0.26 MPa) at 80 °C. Figure 3 shows the optical micrographs of the specimens before and after exposure to the simulated solutions up to 1008 h. The magnification was 100×. Figure 3(a–i) displays the morphological changes in the specimen surface when the dead weight loads were applied. Figure 3(j–m) displays the morphologies of the specimen side surface when the side surface was in contact with test solution all of the time. Figure 3(a–e) presents the surface morphologies of the specimens before and after exposure to the RS or ADT solution for 336 and 1008 h, respectively. Figure 3(f–i) shows the surface morphologies of the specimens after exposure to ADT solution for 336 and 1008 h and after they were subjected to compression loads of 0.13 and 0.26 MPa, respectively.

The optical micrographs in Figure 3(a–c) show the typical surface conditions for the specimens before and after exposure to RS for 336 and 1008 h. The specimens had a smooth surface

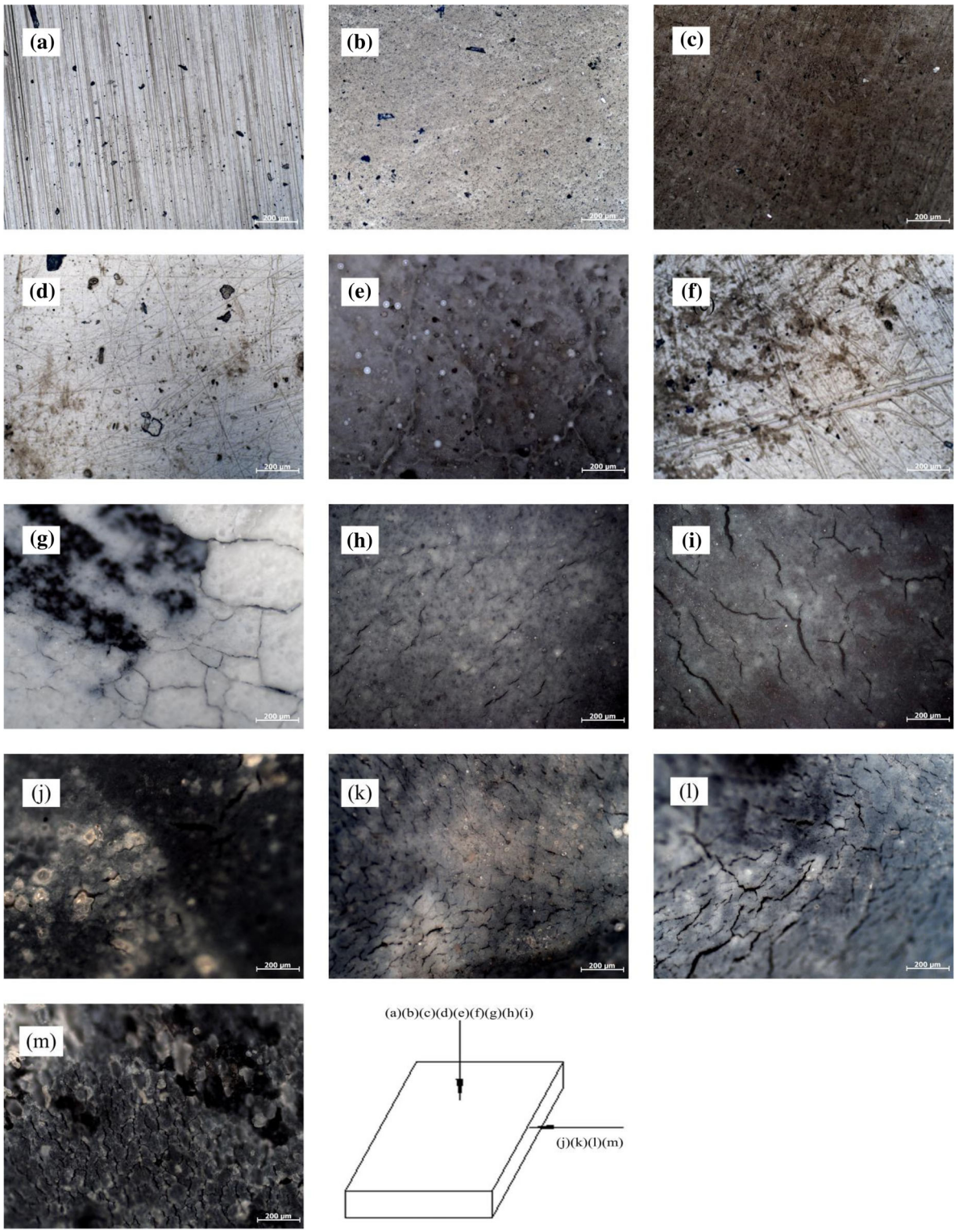

Figure 3. Optical micrographs of the surfaces of the test specimens: (a) before exposure; (b,c) after exposure to the RS for 336 and 1008 h, respectively; (d,e) after exposure to the ADT solution for 336 and 1008 h, respectively; (f,g) after exposure to the ADT solution for 336 and 1008 h, respectively, under 0.13 MPa; (h,i) after exposure to the ADT solution for 336 and 1008 h, respectively, under 0.26 MPa; (j,k) after exposure to ADT for 336 and 1008 h, respectively; and (l,m) after 1008 h of exposure to ADT under 0.13 and 0.26 MPa, respectively. [Color figure can be viewed at wileyonlinelibrary.com]

[see Figure 3(a)] before exposure, and the surface of the specimens became slightly rough after exposure to the RS environment [see Figure 3(c)]. However, no voids or cracks were observed; this indicated that the surface damage of the specimen was not obvious, and the silicone rubber was still stable for specimens exposed to the RS environment for up to 1008 h.

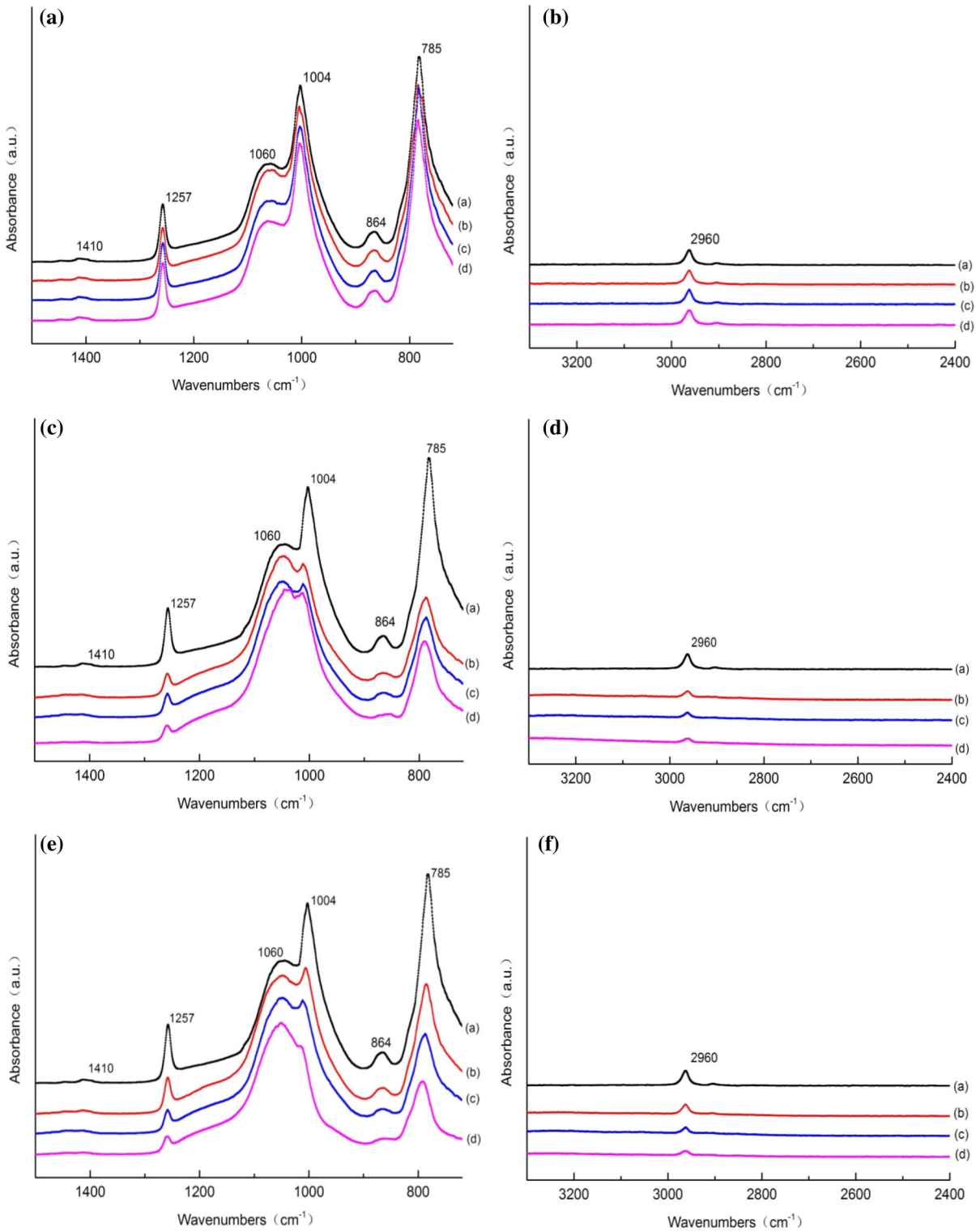

Figure 4. ATR–FTIR test results for the specimens. (A,B) (a) before exposure and (b–d) after exposure to the RS for 672 h at 80 °C under 0, 0.13, and 0.26 MPa, respectively. (C,D) (a) before exposure and (b–d) after exposure to the ADT solution for 672 h at 80 °C under 0, 0.13, and 0.26 MPa, respectively (E,F) (a) before exposure and (b–d) after exposure to the ADT solution under a 0.13 MPa compressive load at 80 °C for 336, 672, and 1008 h, respectively. [Color figure can be viewed at wileyonlinelibrary.com]

Figure 3(d,e) displays the surface morphologies of the specimens after exposure to the ADT solution for 336 and 1008 h. We observed that some corrosion spots appeared after exposure for 336 h [see Figure 3(d)]. The surface of the sample became rougher and some channels were clear after exposure for 1008 h [see Figure 3(e)]. The result indicates that the stability of the silicone rubber material

decreased with increasing acid concentration of the simulated solution [see Figure 3(d,e) for the ADT solution and Figure 3(b,c) for the RS].

Figure 3(f,g) shows the surface morphology of the specimens after exposure to the ADT solution for 336 and 1008 h and after it was subjected to the 0.13 MPa compression load. Some deep channels appeared on the surface after 336 h of exposure [see Figure 3(f)], and cracks initiated and propagated after 1008 h of exposure [see Figure 3(g)].

Figure 3(h,i) shows the surface morphologies of the specimens after exposure to the ADT solution for 336 and 1008 h and after they were subjected to the 0.26 MPa compression load. The cracks initiated on the surface of specimen after 336 h of exposure [see Figure 3(h)], and the cracks became more severe with increasing exposure time [see Figure 3(i)].

Figure 3(j,k) presents the typical morphologies on the side surfaces of the specimens after exposure to the ADT solution for 336 and 1008 h. Figure 3(l,m) displays the typical morphologies on the side surfaces of the specimens after exposure to the ADT solution for 1008 h and after being subjected to the 0.13 and 0.26 MPa compression loads. The cracks were deeper and denser with increasing compression load [see Figure 3 (k–m)]. In addition, the side-surface degradation of the specimens [see Figure 3 (k–m)] were more severe under identical conditions because the surface was in direct contact with the test solution.

On the basis of the optical microscopy results, the following conclusions were made:

1. The surface morphological changes in the specimen showed that the exposure time affected the damage of the specimen.
2. Both the acid concentration and compression load had significant effects on the surface degradation, and the damage was more severe under higher acidic concentrations or with a greater compression load.

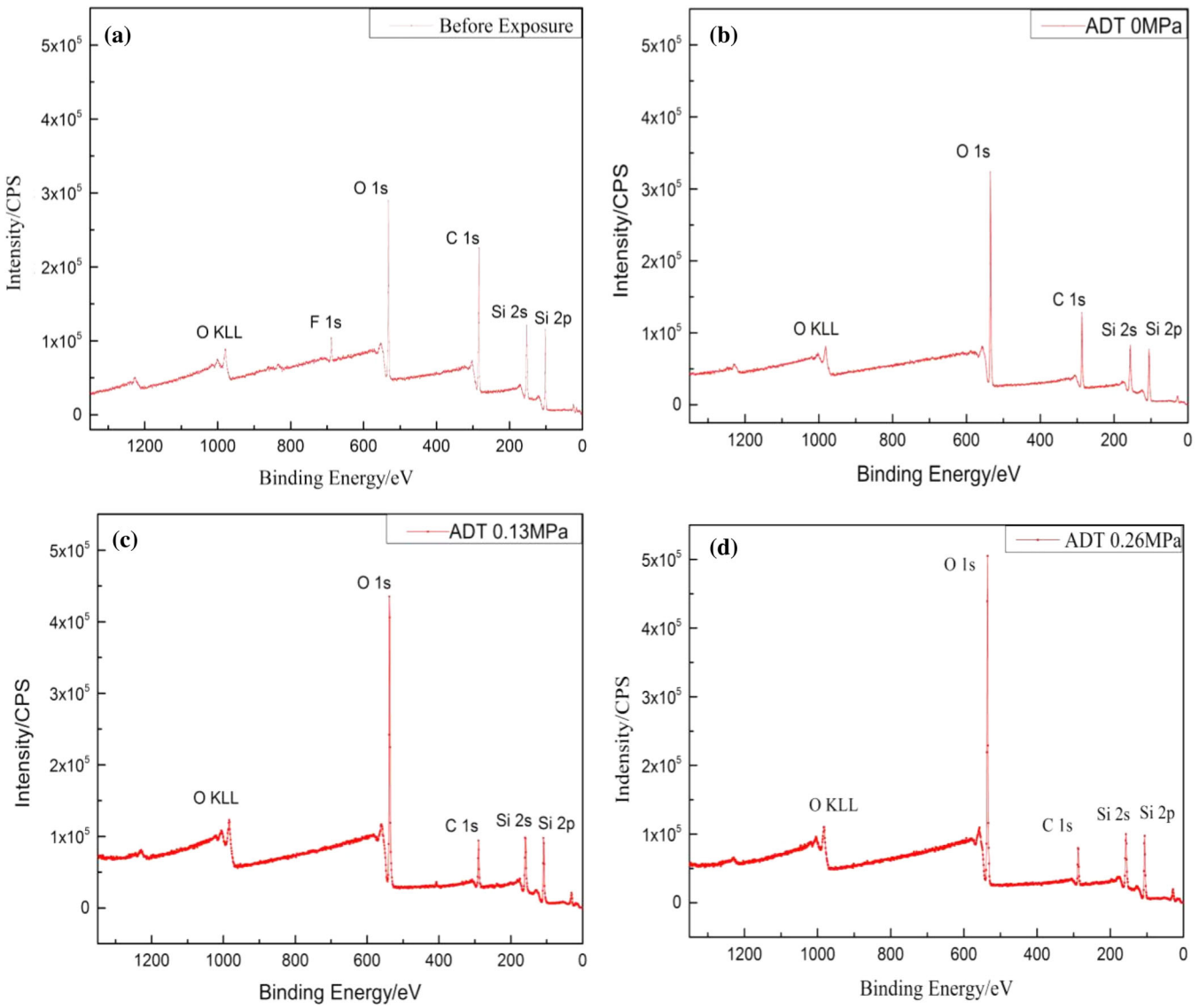

Figure 5. Surface XPS survey spectra for the silicone rubber specimens before and after exposure to the ADT solution: (A) before exposure, (B) after 672 h of exposure, (C) after 672 h of exposure under 0.13 MPa, and (D) after 672 h of exposure under 0.26 MPa: (KLL) Auger peak of O (Oxygen) element and (CPS) Counts per Second. [Color figure can be viewed at wileyonlinelibrary.com]

Table I. Surface Atomic Concentrations of C, O, Si, and F and Ratios of the Atomic Concentrations of C and O to Si for the Silicone Rubber Specimens before and after Exposure to ADT Solutions under Different Compression Loads

	Atomic concentration (atom %)				Ratio to Si	
Sample	C	O	Si	F	C/Si	O/Si
Before exposure	46.13	25.49	27.74	0.64	1.663	0.919
672 h of exposure in ADT	30.67	37.36	31.64	0.34	0.821	1.054
672 h of exposure in ADT under 0.13 MPa	19.65	46.7	33.32	0.33	0.590	1.402
672 h of exposure in ADT under 0.26 MPa	16.82	47.8	35.08	0.3	0.480	1.363

3. The side-surface damage of the silicone rubber specimen was more severe when the surface was always in contact with compression load under identical conditions.

ATR–FTIR Spectroscopy

To investigate the chemical changes in the silicone rubber specimens after exposure to simulated solutions and compressive loads, ATR–FTIR analysis was conducted, and the ATR–FTIR spectra are shown in Figure 4. Figure 4(A,B) displays the ATR–FTIR spectra of the specimens after exposure to the RS and various compression stresses (i.e., 0.13 or 0.26 MPa) at 80 °C for 672 h. Figure 4(C,D) displays the ATR–FTIR spectra of the specimens after exposure to the ADT solution and various compression stresses (i.e., 0.13 or 0.26 MPa) at 80 °C for 672 h. Figure 4(E,F) displays the ATR–FTIR spectra of the specimens after exposure to the ADT solution and to 0.13 MPa compression stress for 336, 672, and 1008 h, respectively. For comparison, the spectra of the unexposed specimens are shown in Figure 4.

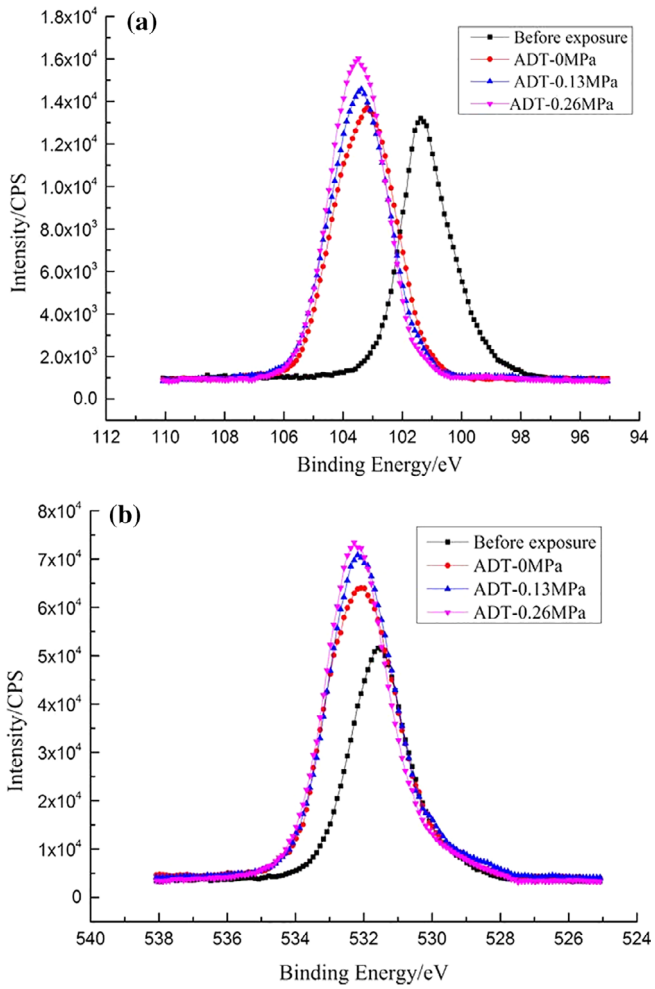

Figure 6. High-resolution spectra for the specimens of (a) Si2p under different compressive loads after exposure for 672 h and (b) O1s under different compression loads after exposure for 672 h: (CPS) Counts per Second. [Color figure can be viewed at wileyonlinelibrary.com]

For unexposed specimens, the broadest and strongest peak appeared between 1004 and 1060 cm^{-1} [see Figure 4(A-a,C-a,E-a)]. Other peaks were observed at 785, 864, 1257, 1410, and 2960 cm^{-1}, respectively. The peaks appeared at 1004–1060 cm^{-1} because of the stretching vibrations of the Si—O—Si chain on the silicone rubber. The peak at 785 cm^{-1} was assigned to the coupled stretching vibrations of Si—C and the rocking vibrations of —CH_3. The peaks at 864 and 1257 cm^{-1} were assigned to the bending vibrations and rocking vibrations of the Si—CH_3 group. The peak at 1410 cm^{-1} was assigned to the rocking vibrations of —CH_2— group. The peak at 2960 cm^{-1} was assigned to the stretching vibrations of the CH_3 group. For the relationship between the wave number and vibration mode, refer to the handbook in ref. 28.

For specimens exposed to the RS environment for 672 h and subjected to compression loads (i.e., 0.13 and 0.26 MPa), the intensity of the characteristic peaks did not change [see Figure 4(A,B)]; this indicated that the chemical structure of the specimen surface did not change after exposure to the RS environment and the compression load (i.e., 0.13 or 0.26 MPa).

For specimens exposed to ADT solution for 672 h and compression loads (i.e., 0.13 and 0.26 MPa), the characteristic peaks between 1004 and 1060 cm^{-1} and at 785, 864, 1410, 1257, and 2960 cm^{-1} decreased sharply, especially the peaks between 1004 and 1060 cm^{-1} [see Figure 4(C-b,D-b)]. As also shown in Figure 4(C,D), the intensity of all of the characteristic peaks decreased gradually with increasing compression load. The peaks at 1257 and 2960 cm^{-1} decreased gradually under the compression loads (from 0.13 to 0.26 MPa), and the peaks at 1410 and 864 cm^{-1} almost disappeared under the 0.26 MPa compression load after 672 h of exposure.

For specimens exposed to the ADT solution and subjected to a 0.13 MPa compression load for up to 1008 h [see Figure 4(E,F)], the intensity of all of the characteristic peaks decreased with exposure time. The peaks at 1410 and 864 cm^{-1} almost disappeared after exposure for 1008 h [see Figure 4(E-d,F-d)].

For specimens in RS and those subjected to compression loads, the characteristic peaks almost did not change [see Figure 4(A,B)]. However, after the specimens were exposed to the ADT solution and different compression loads, the intensity of the characteristic peaks changed significantly [see Figure 4(C,D)] and decreased with increasing compression load. The results indicate that both the concentration of the acidic solution and the compression load significantly affected the chemical damage to the silicone rubber specimens; the specimens degraded more under higher acidic concentrations and with more compression stress. The ATR–FTIR test results were consistent with those from the weight loss measurements.

From the ATR–FTIR study, we concluded that the backbone (Si—O—Si) and crosslink domain (CH_2) seriously changed for the specimens exposed to the simulated solutions (especially the ADT solution) and subjected to compressive loads over time. The chemical change in silicone rubber could have mainly been due to the attack of Si—O—Si to form Si—OH by strong acid. The formed Si—OH groups could be converted to Si—O. The compression load accelerated this reaction. Although the Si—O—Si chain was stable, it could also be destroyed in a strongly acidic solution and under compression loads. The destruction of the Si—O—Si chain caused the chemical degradation of the silicone rubber material.[26,29,30]

XPS

XPS analysis was conducted to study the degradation mechanism of the silicone rubber material after exposure to the simulated environments and the compression loads.

Figure 5(A,B) displays the XPS survey spectra for the specimens before and after exposure to the ADT solution for 672 h at 80 °C. Figure 5(C,D) presents the XPS survey spectra for specimens exposed to the ADT solution and the compression stresses (i.e., 0.13 and 0.26 MPa) for 672 h at 80 °C. In Figure 5, the O KLL represents Auger peak of Oxygen (O) element, CPS presents counts per second.

As shown in Figure 5(A–D), silicon (Si), oxygen (O), carbon (C), and fluorine (F) were present in the spectra. The atomic concentrations of the four elements on the specimen surface are shown

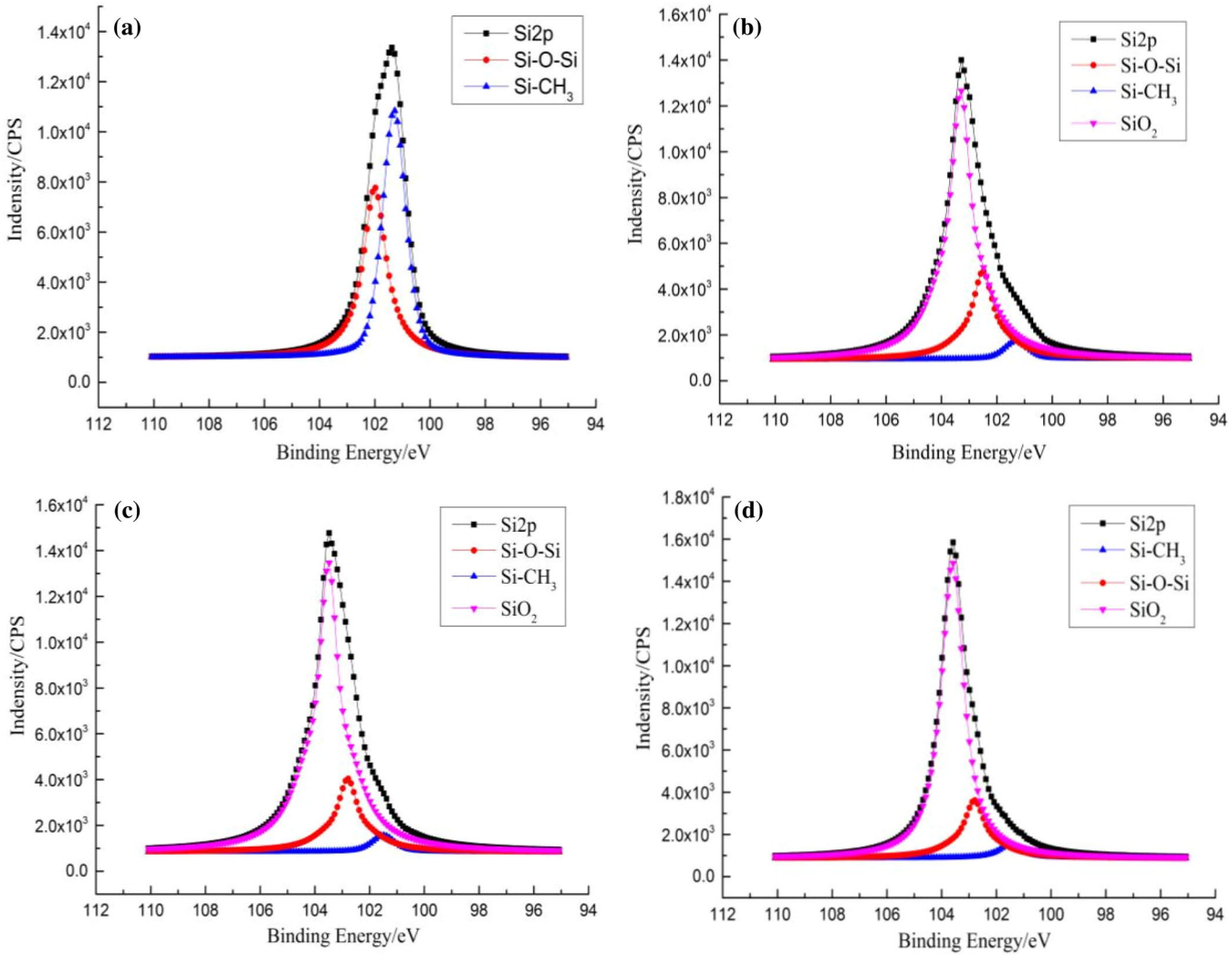

Figure 7. High-resolution spectra of Si2p for the specimens (a) before exposure and (b–d) after exposure to the ADT solution for 672 h under 0, 0.13, and (d) 0.26 MPa: (CPS) Counts per Second. [Color figure can be viewed at wileyonlinelibrary.com]

in Table I. As shown clearly in Figure 5(A,B), the peak of C1s obviously decreased, whereas the peak of O1s increased after the specimen was exposed to the ADT solution for 672 h. For the specimen exposed to the ADT solution and subjected to the 0.13 MPa compression load, the peak intensities of C1s and O1s changed significantly [see Figure 5(B,C)]. As shown in Table I, we found that with increasing compression load and exposure time, the C/Si proportion decreased, whereas the O/Si proportion increased. This was mainly due to the destruction of the methyl group on the silicone atoms and the formation of Si—O bonds as well as the hydrolysis of the crosslinked regions (C—C bonds and Si—C bonds). The increase in the O/Si ratio indicated that the —Si—O—Si— chain was attacked and destroyed for the specimen exposed to the simulated environments and subjected to compression loads over time.

To further study the damage process mechanism of the specimen after exposure to simulated environments and compression loads, high-resolution XPS analysis was performed. The Si2p high-resolution spectra of the specimen before and after exposure to the ADT solution for 672 h and to the 0.13 and 0.26 MPa compression loads are presented in Figure 6(a). Figure 6(a) shows that the binding energy of Si2p shifted about 2.5 eV to a higher binding energy level for the specimens exposed to the ADT solution for 672 h. The intensity of the characteristic peak also increased. For specimens exposed to the ADT solution and to the 0.13 or 0.26 MPa compression load, the trends in the peak change were similar to those of the specimen after exposure to the ADT solution without a compression load. The O1s high-resolution spectra of the specimen before and after exposure to the ADT solution for 672 h and those subjected to the 0.13 and 0.26 MPa compression loads are shown in Figure 6(b). The intensity of the characteristic peak showed a significant increase for the specimens exposed to the ADT solution for 672 h. The binding energy of O1s shifted approximately 1 eV toward a higher binding energy level. The intensity of the characteristic peak for specimens exposed to the ADT solution and subjected to a 0.13 or 0.26 MPa compression load increased obviously compared to

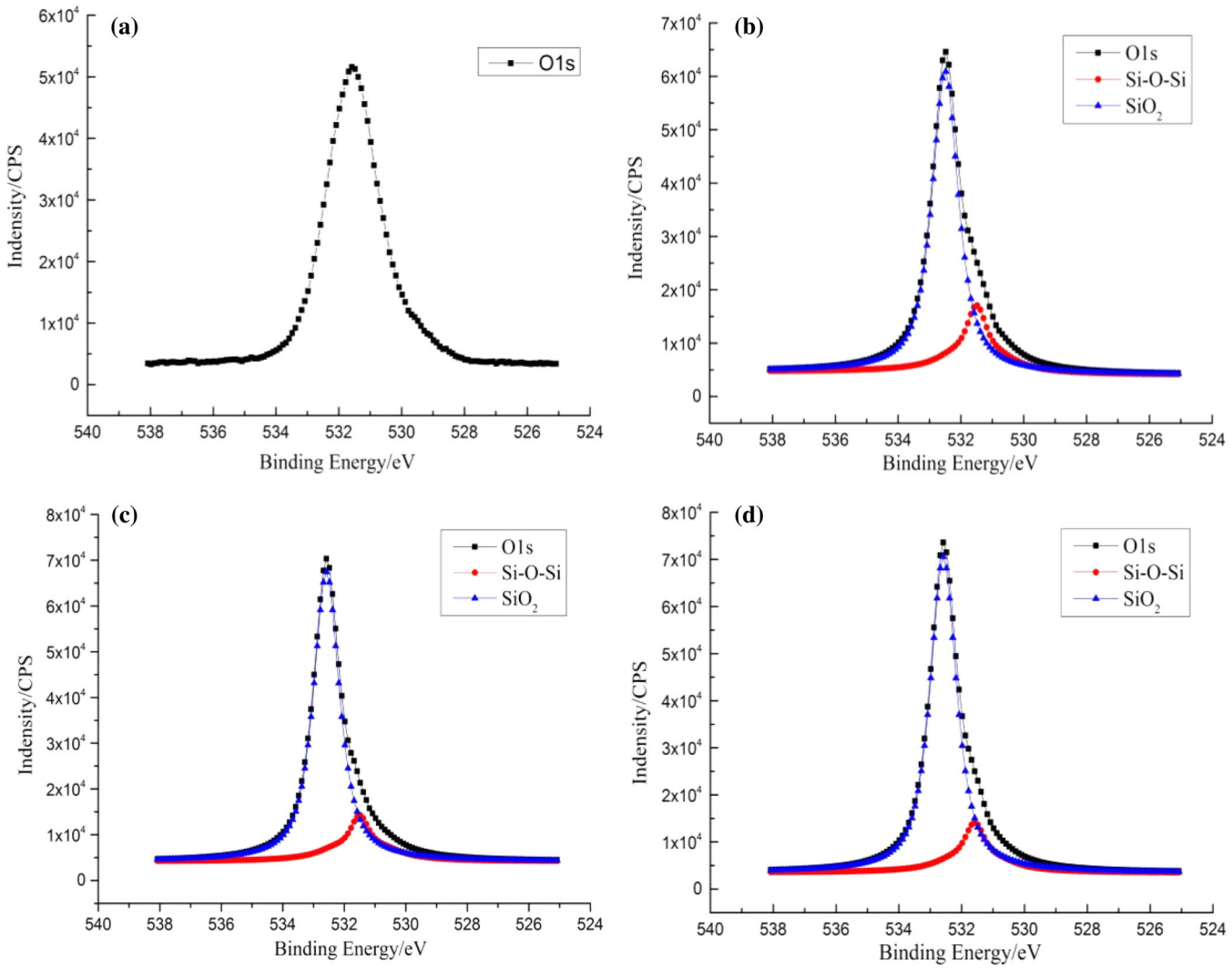

Figure 8. High-resolution spectra of O1s for the specimens (a) before exposure and (b) after exposure to the ADT solution for 672 h under 0, 0.13, and 0.26 MPa, respectively: (CPS) Counts per Second. [Color figure can be viewed at wileyonlinelibrary.com]

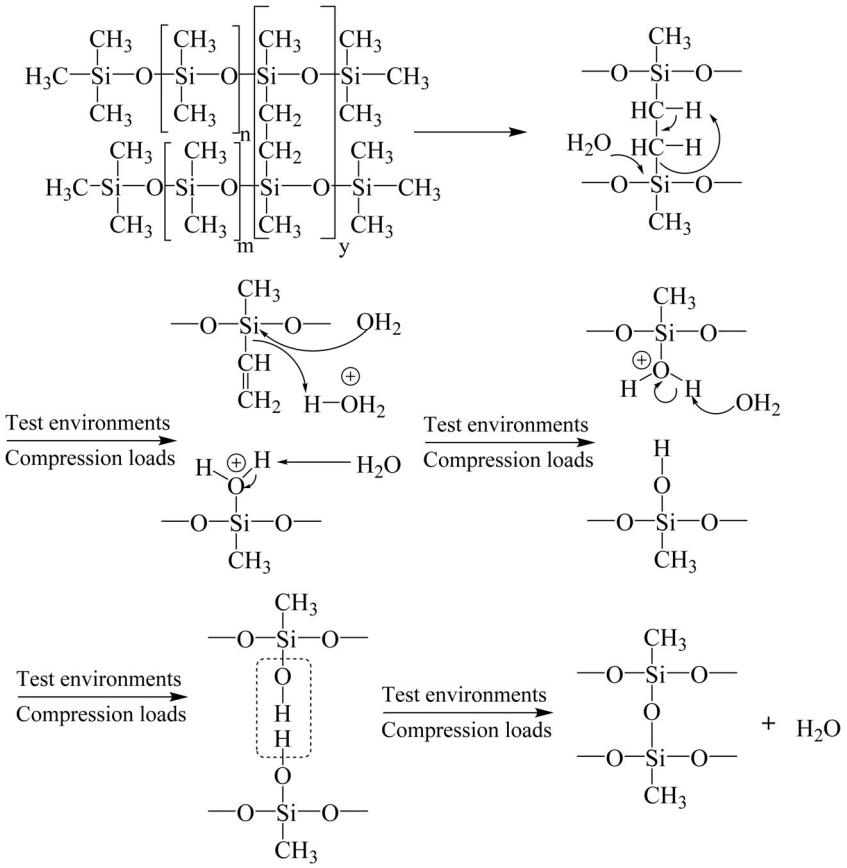

Scheme 1. Decrosslinking reaction at the crosslinked sites of the rubber and combination reaction.

that of the unexposed specimen. The results indicate that for the specimens exposed to the ADT solution and subjected to the compression loads, the surface showed important chemical changes; that is, the main chain (—Si—O—Si—) of the specimen degraded to produce Si—O bonds.

To further understand the chemical changes and degradation mechanisms for the silicone rubber specimens after exposure, the peak-differentiation-imitating method was used to analyze the specimens in the Si2p and O1s regions. The XPS peak-differentiation-imitating results of the spectra for specimens after exposure to the ADT solution and under 0.13 and 0.26 MPa compression loads for 672 h are shown in Figures 7 and 8, respectively. Figure 7 shows the high-resolution spectra of Si2p for the specimens before and after exposure to the ADT solution for 672 h without load and with compression loads of 0.13 and 0.26 MPa. Figure 8 presents the high-resolution spectra of O1s for the specimens before exposure and after exposure to the ADT solution for 672 h without load and with compression loads of 0.13 and 0.26 MPa.

The curve-fitting results of the Si2p spectra for the specimens before and after exposure to the ADT solution and after subjection to different compression loads (i.e., 0.13 and 0.26 MPa) are presented in Figure 7(a–d), respectively. Figure 7(a,b) shows the curve-fitting results of the Si2p spectra for the specimens before exposure and after exposed to the ADT solution for 672 h. Figure 7(c,d) shows the curve-fitting results of the Si2p spectra for specimens after exposure to the ADT solution and after subjection to compression loads of 0.13 and 0.26 MPa. As shown in Figure 7(a), we found that the characteristic peak of Si2p contained two single peaks for the specimen before the exposure. The first peak, at a binding energy of 102 eV, corresponded to the main-chain Si—O—Si bonds.[31] The other peak, at a binding energy of 101.3 eV, corresponded to the Si—CH_3[31] bonds and was connected with the side group. For the specimen exposed to the ADT solution for 672 h without a compression load, a new characteristic peak appeared at a binding energy of 103.5 eV [see Figure 7(b)]; this was related to a new group (SiO_2)[31] on the specimen surface. However, the peaks at 102 and 101.3 eV decreased significantly. After the samples were exposed to the ADT solution for 672 h under a 0.13 or 0.26 MPa compression load, the Si2p spectra [see Figure 7(c,d)] were similar to the XPS spectra shown in Figure 7(b). However, the intensities of the characteristic peak at 102 eV corresponding to the Si—O—Si structure and the peak at 101.3 eV corresponding to Si—CH_3 structure decreased, whereas the intensity of the characteristic peak at 103.5 eV corresponding to SiO_2 increased. The results demonstrate that when the specimen was exposed to the ADT solution and subjected to compression loads for up to 672 h, the Si—O—Si structure on the specimen surface was destroyed, and new material (i.e., SiO_2) was produced. In addition, with increasing compression load, the main-chain Si—O—Si structure and side-chain Si—CH_3 structure gradually decreased, and the new material SiO_2 increased gradually. This showed that the samples degraded more seriously with increasing compression load.

The curve-fitting results of the O1s spectra for specimens exposed to the ADT solution and subjected to 0.13 MP and 0.26 MPa compression loads are shown in Figure 8(a–d), respectively.

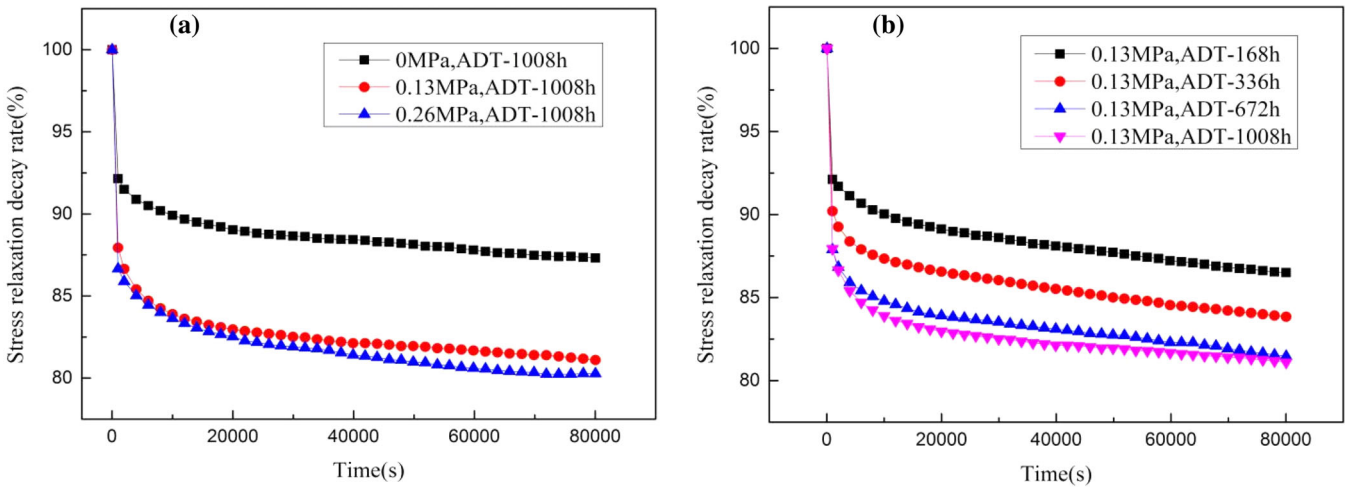

Figure 9. Normalized stress-relaxation curves of the silicone rubber samples at an initial strain of 25%: (a) after exposure to the ADT solution for 1008 h and subjection to compression loads of 0.13 and 0.26 MPa and (b) after exposure to the ADT solution and subjection to a compression load of 0.13 MPa for 168, 336, 672, and 1008 h. [Color figure can be viewed at wileyonlinelibrary.com]

Figure 8(a,b) shows the curve-fitting results of the O1s spectra for specimens before and after exposure to the ADT solution for 672 h. Figure 8(c,d) shows the curve-fitting results of the Si2p spectra for the specimens after exposure to the ADT solution for 672 h and compression loads of 0.13 and 0.26 MPa. As shown in Figure 8(a), before the specimen was exposed to the ADT solution, the O1s XPS spectrum was fitted by only one peak; this corresponded to the Si—O—Si bonds. After the specimen was exposed to the ADT solution for 672 h without a compression load, the O1s XPS spectrum was fitted by two characteristic peaks (i.e., at 531.5 and 532.5 eV binding energies). The newly generated characteristic peak at a binding energy of 532.5 eV [see Figure 8(b)] corresponded to the production of new material (SiO_2).[31] As shown in Figure 8(b), the intensity of the characteristic peak corresponding to SiO_2 obviously increased, and the peak corresponding to Si—O—Si decreased sharply. This change demonstrated that for the specimen exposed to the ADT solution for up to 672 h, the degradation process was mainly due to the main-chain Si—O—Si backbone fractured and accompanied with SiO_2 generation. The O1s spectra shown in Figure 8(c,d) were similar to the spectra shown in Figure 8(b).

Moreover, with increasing compression loads [see Figure 8(c,d)], the intensity of characteristic peak at 531.5 eV corresponding to the Si—O—Si structure decreased gradually, whereas the peak at 532.5 eV corresponding to SiO_2 increased gradually. The results show that the damage process was mainly caused by the breaking of the main-chain Si—O—Si structure and was accompanied by the formation of SiO_2; the surface of the silicone rubber samples was degraded more severely by strong acid and a greater compression load. The O1s analysis results were consistent with the Si2p results.

The chemical composition changes in the silicone rubber material indicated that the specimens showed obvious chemical damage after exposure to the test solution and the compression loads (i.e., 0.13 and 0.26 MPa). The degradation of silicone rubber material may have affected not only the sealing performance as gaskets but also the durability and lifetime of the fuel cells.[12,15] The XPS experimental results were consistent with the FTIR spectroscopy conclusions.

We concluded from the ATR–FTIR and XPS study that the backbone of silicone rubber and the crosslinked domain for the specimens obviously changed chemically over time. The degradation mechanisms of the silicone rubber mainly proceeded via decrosslinking and chain scissoring in the backbone. The most likely decrosslinking reactions at the crosslink positions of the silicone rubber and combination reactions after exposure to the test environments are shown in Scheme 1. At the crosslinking sites, there existed bonds of C—C, C—H, and C—Si (see Scheme 1). Because the Si—C bond had the lowest dissociation energies,[32] the chemical change in the silicone rubber crosslinked domain was most likely due to the damage to Si—C through hydrolysis to form Si—OH, as shown in Scheme 1. After prolonged exposure to the test environments, the Si—OH groups were combined to form the new Si—O—Si, and this process is also shown in Scheme 1.

Compression Stress-Relaxation Test

To elucidate the compression mechanical properties of the silicone rubber material, compression stress-relaxation measurements, as an important characterization method of the compression mechanical properties, were used in this study. Figure 9 shows the test results of the compression stress relaxation obtained from a strain level of 25% for the samples after exposure to the ADT solution and the compression loads. The tests were performed in an ambient air environment and terminated after 80,000 s when the stress-relaxation rate gradually tended toward their equilibrium state.

Figure 9(a) presents the normalized stress-relaxation curves after 1008 h of exposure to the ADT solution and after subjection to the 0.13 and 0.26 MPa compression loads. As shown in Figure 9 (a), the stress relaxed sharply at the beginning; then, the stress decreased gradually with time and finally reached an equilibrium. The stress relaxation of the silicone rubber samples without

compression load was slower than that of the samples subjected to a 0.13 or 0.26 MPa compression load under an identical exposure time of 1008 h. These behaviors indicate that the compression load had a significant influence on the compression stress-relaxation properties: the greater the compressive load was, the faster the samples relaxed. Figure 9(b) presents the normalized stress relaxation with time after the specimens were exposed to the ADT solution under a 0.13 MPa compression load for 168, 336, 672, and 1008 h, respectively. We observed that the compression stress-relaxation decay rate decreased with the exposure time; that is, the curves attenuated more with a greater exposure time. The results show that the exposure time also significantly affected the sample stress-relaxation decay rate.

CONCLUSIONS

The degradation processes and mechanisms of silicone rubber material exposed to two environments and subjected to two compression loads were investigated in this study. The obtained conclusions were as follows:

1. The weight loss test results indicate that both test solutions, the exposure time, and the compression load had great influences on the weight loss of the silicone rubber specimens. The specimen lost more weight when a larger compression load was applied and when it was exposed to a solution with a higher acidic concentration.
2. Optical microscopy showed that the surface morphologies of the specimens changed. The surface morphology changed from smooth to rough; this was followed by crack appearance and, finally, crack propagation. The surface damage became more severe when the sample was exposed to a solution with a higher acidic concentration and when it was subjected to a greater compression stress.
3. The ATR–FTIR and XPS results reveal that the chemical structure of the silicone rubber changed greatly after the specimen was exposed to simulated environments and subjected to compression loads, and the specimen degraded more severely in strong acid solutions and when greater compression loads were applied. The degradation mechanism could have been chain scissoring in silicone rubber and the hydrolysis of the crosslinking positions.
4. The compression stress-relaxation measurements results indicate that the stress-relaxation properties of the silicone rubber specimens changed significantly for the specimens exposed to the test environments and subjected to the compression loads. The chemical damage and compression loads had a great influence on the mechanical properties of specimen.
5. The results of this study show the chemical and mechanical degradation process and mechanism of silicone rubber after exposure to the test solutions and compression loads. The chemical and mechanical degradation of silicone rubber gaskets may affect the electrochemical performance of the fuel cell. Investigations on the durability and electrochemical performance of PEM fuel cells during operation with damaged silicone rubber gaskets are under study. The results will be reported later.

ACKNOWLEDGMENTS

This work was sponsored by the Natural Science Foundation of China (contract grant number 51175241).

REFERENCES

1. Wu, H. W. *Appl. Energy*. **2016**, *165*, 81.
2. Gonnet, A. E.; Robles, S.; Moro, L. *Int. J. Hydrogen Energy*. **2012**, *37*, 14757.
3. Liang, P.; Qiu, D.; Peng, L.; Yi, P.; Lai, X.; Ni, J. *Int. J. Hydrogen Energy*. **2017**, *42*, 10217.
4. Chen, H.; Pei, P.; Song, M. *Appl. Energy*. **2015**, *142*, 154.
5. St-Pierre, J. *Int. J. Hydrogen Energy*. **2011**, *36*, 5527.
6. Uddin, M. A.; Qi, J.; Wang, X.; Pasaogullari, U.; Bonville, L. *Int. J. Hydrogen Energy*. **2015**, *40*, 13099.
7. Pehlivan-Davis, S.; Clarke, J.; Armour, S. *J. Appl. Polym. Sci.* **2013**, *129*, 1446.
8. Schulze, M.; Knöri, T.; Schneider, A.; Gülzow, E. *J. Power Sources*. **2004**, *127*, 222.
9. Mitra, S.; Ghanbari-Siahkali, A.; Kingshott, P.; Rehmeier, H. K.; Abildgaard, H.; Almdal, K. *Polym. Degrad. Stab.* **2006**, *91*, 69.
10. Mitra, S.; Ghanbari-Siahkali, A.; Kingshott, P.; Rehmeier, H. K.; Abildgaard, H.; Almdal, K. *Polym. Degrad. Stab.* **2006**, *91*, 81.
11. Kim, J. K.; Kim, I. H. *J. Appl. Polym. Sci.* **2001**, *79*, 2251.
12. Feng, J.; Zhang, Q.; Tu, Z.; Tu, W.; Wan, Z.; Pan, M.; Zhang, H. *Polym. Degrad. Stab.* **2014**, *109*, 122.
13. Li, K.; Zhang, H.; Pan, M. *Rubber Chem. Technol.* **2015**, *88*, 475.
14. Chang, H.; Wan, Z.; Chen, X.; Wan, J.; Luo, L.; Zhang, H.; Tu, Z. *Appl. Therm. Eng.* **2016**, *104*, 472.
15. Cui, T.; Chao, Y. J.; Van Zee, J. W. *Int. J. Hydrogen Energy*. **2012**, *37*, 13478.
16. Cui, T.; Chao, Y. J.; Chen, X. M.; Van Zee, J. W. *J. Power Sources*. **2011**, *196*, 9536.
17. Cui, T.; Lin, C. W.; Chien, C. H.; Chao, Y. J.; Van Zee, J. W. *J. Power Sources*. **2011**, *196*, 1216.
18. Kim, M. S.; Kim, J. H.; Kim, J. K.; Kim, S. J. *Macromol. Res.* **2007**, *15*, 315.
19. Tan, J.; Chao, Y. J.; Van Zee, J. W.; Li, X.; Wang, X.; Yang, M. *Mater. Sci. Eng. A*. **2008**, *496*, 464.
20. Tan, J.; Chao, Y. J.; Wang, H.; Gong, J.; Van Zee, J. W. *Polym. Degrad. Stab.* **2009**, *94*, 2072.
21. Tan, J.; Chao, Y. J.; Yang, M.; Lee, W. K.; Van Zee, J. W. *Int. J. Hydrogen Energy*. **2011**, *36*, 1846.
22. Rey, T.; Chagnon, G.; Le Cam, J. B.; Favier, D. *Polym. Test.* **2013**, *32*, 492.
23. Li, G.; Tan, J.; Gong, J. *J. Power Sources*. **2012**, *217*, 175.
24. Liu, J.; Wu, S.; Dong, E. *J. Appl. Polym. Sci.* **2013**, *128*, 2337.
25. Millichamp, J.; Mason, T. J.; Neville, T. P.; Rajalakshmi, N.; Jervis, R.; Shearing, P. R.; Brett, D. J. *J. Power Sources*. **2015**, *284*, 305.

26. Tan, J.; Chao, Y. J.; Li, X.; Van Zee, J. W. *J. Power Sources*. **2007**, *172*, 782.

27. Han, X.; Tan, J.; Liu, Y. *Acta Energiae Solaris Sinica*. **2017**, *37*, 2978 (in Chinese).

28. Lin-Vien, D.; Colthup, N. B.; Fateley, W. G.; Grasselli, J. G. The Handbook of Infrared and Raman Characteristic Frequencies of Organic Molecules; Elsevier: Amsterdam, **1991**.

29. Yoshimura, N.; Kumagai, S.; Nishimura, S. *IEEE Trans. Dielectrics Electrical Insulation*. **1999**, *6*, 632.

30. Delor-Jestin, F.; Tomer, N. S.; Singh, R. P.; Lacoste, J. *Sci. Technol. Adv. Mater*. **2008**, *9*, 024406.

31. Moulder, J. F.; Stickle, W. F.; Sobol, P. E.; Bomben, K. D. Handbook of X-Ray Photoelectron Spectroscopy: A Reference Book of Standard Spectra for Identification and Interpretation of XPS Data; PerkinElmer: Eden Prairie, MN, **1992**.

32. Streiwieser, A., Jr.; Heathcock, C. H. Introduction to Organic Chemistry; Macmillan: New York, **1976**.